

# On the optimum distance for signal-energy mapping in extensive air shower arrays

G. Ros<sup>a</sup>, G. Medina-Tanco<sup>b</sup>, L. del Peral<sup>a</sup>, J. C. D'Olivo<sup>b</sup>,  
F. Arqueros<sup>c</sup>, M. D. Rodríguez-Frías<sup>a</sup>.

<sup>a</sup>*Space Plasmas and Astroparticle Group, Dpto. Física, Universidad de Alcalá  
Ctra. Madrid-Barcelona km. 33. Alcalá de Henares, E-28871 (Spain).*

<sup>b</sup>*Instituto de Ciencias Nucleares, UNAM, Circuito Exterior S/N, Ciudad  
Universitaria, México D. F. 04510, México.*

<sup>c</sup>*Dpto. Física Atómica, Molecular y Nuclear, Facultad de Física, Universidad  
Complutense de Madrid, Ciudad Universitaria 28040, Madrid (Spain).*

---

## Abstract

In high energy cosmic rays surface arrays, the primary energy is currently determined from the value of the lateral distribution function (LDF) at a fixed optimum distance  $r_{opt}$  from the shower core. The value of  $r_{opt}$  is mainly related to the geometry of the array and is, therefore, considered as fixed independently of the shower energy or direction. Here, we demonstrate that the dependence of  $r_{opt}$  on energy and zenith angle is not negligible. As a consequence, this method may not reconstruct properly the shape of the spectrum and might change the position of spectral features like the ankle. This result applies for pure surface array experiments but not to hybrid experiments, like the Pierre Auger Observatory, where hybrid events are used to calibrate the reconstructed energy of surface events. Additionally, events with saturated stations must be either properly corrected or eliminated altogether from the analysis when applying the  $r_{opt}$  method. We show that calculating a specific  $r_{opt}$  on a shower-to-shower bases, instead of using a fixed value, may avoid the problem of events with saturated stations and improve, at the same time, the reconstruction of spectral features.

---

<sup>0</sup> G. Ros: Tel/fax: +34-918854954/42. E-mail address: german.ros@uah.es. In collaboration with Universidad Complutense de Madrid and Universidad Nacional Autónoma de México.

## 1 Introduction

The energy spectrum of cosmic rays is observed from energies below 1 GeV up to more than  $10^{20}$  eV. Different experiments are involved in its determination at different energy ranges. At high enough energies, when extensive air showers (EAS) develop into the atmosphere, two different experimental approaches have been traditionally used. The first one consists on the inference of the particle lateral distribution function (LDF) from the discrete sampling of the shower front at ground level by a surface array of detectors. Mainly scintillators (e.g., Volcano Ranch, AGASA, KASCADE) and water Cherenkov detectors (e.g., Haverah Park) have been customarily used to this end. The second approach consists on the reconstruction of the longitudinal profile of the shower from the fluorescence light produced by atmospheric Nitrogen as it is excited by charged EAS particles along the atmosphere (e.g., Fly's Eye, HiRes). The latter is considered to be the nearest thing to a calorimetric measurement of the primary cosmic ray particle energy.

A special case from the experimental point of view is the Pierre Auger Observatory [1] which pioneers the simultaneous use of both techniques, water Cherenkov detectors and fluorescence telescopes, for roughly 10% of the incoming events. For these so called hybrid events, the systematic errors in their energy estimate are greatly reduced.

The estimation of the shower energy from the surface detector array is a two step process. First, the LDF of the shower particles, i.e. the particle density or signal versus distance to the shower core location, is fitted assuming a known functional form. This fit suffers from uncertainties related to the statistical shower fluctuations, the uncertainties in core location and the ignorance of the exact form of the LDF. The normalization constant of the LDF of an extensive air shower is a monotonous (almost linear) increasing function of the energy of the primary cosmic ray. Therefore, the interpolated signal at some fixed distance from the core can be calibrated to estimate the shower energy. In order to avoid the large fluctuations in the integral of the signal over all distances, which may cause a large uncertainty in energy estimation, Hillas [2] proposed to use instead the interpolated signal at some fixed optimal distance from the shower core,  $S(r_{opt})$ , which is much more stable. The uncertainty due to the lack of knowledge of the LDF is also minimized with this procedure. The optimum distance  $r_{opt}$  is mainly related to the array geometry, and the same value is used to estimate the energy for all the showers, regardless of their primary energy or direction. AGASA, Yakutsk and Haverah Park choose  $r_{opt} = 600$  m, while Auger uses 1000 m due to its larger array spacing [3]. In the second step, there are at least two possible approaches in order to relate  $S(r_{opt})$  with the primary energy: use either Monte Carlo simulations or, as in the case of Auger [4], the calorimetric measurement obtained from the

fluorescence observation of hybrid events.

We performed a detailed study of  $r_{opt}$  as a function of array spacing, primary energy and zenith angle of the cosmic ray shower and demonstrate that these dependencies are not negligible. Therefore, considering a fixed value for  $r_{opt}$  may introduce errors in the determination of the energy spectrum. As a case study, we use an AGASA-like experiment to process both a single power law energy spectrum and a realistically structured spectrum above  $10^{17.7}$  eV. We reconstruct the injected spectra with the LDF and energy parametrization reported by AGASA [5]. In order to compare the two approximations, we use in the reconstruction process both a fixed  $r_{opt} = 600\text{m}$  – the same used by AGASA – and our own shower-to-shower estimate of the optimum distance. In the former case a special analysis is needed to reconstruct saturated events, while not in the latter method.

Fig. 1 shows the cosmic ray spectrum measured by different experiments. There are three main differences between them. First, AGASA found the so called ankle of the spectrum around  $10^{19}$  eV, in agreement with Yakutsk [6]. However, it has been observed around  $3 \times 10^{18}$  eV by Fly’s Eye [7], Haverah Park [8], HiRes [9] and Auger [4]. Fly’s Eye suggested that the cosmic rays spectrum above  $10^{17}$  eV has two components, a Galactic one with spectral index  $\sim -3.5$  at lower energies and an extragalactic one with index  $\sim -2.6$  which dominates above  $10^{18}$  eV. In fact, some models relate the ankle to the transition between Galactic and extragalactic components [10,11] while others suggest that it is the result of photo-pair creation by proton interactions with the cosmic microwave background [12] (see also [13,14,15,16] for a full discussion). Furthermore, a considerable difference in flux is apparent even after taking into account the energy uncertainties of each experiment. Finally, the spectrum cut off at the higher energies was not observed by AGASA, but HiRes and Auger have confirmed it with more than  $4\sigma$  of significance [9,4].

Section 2 describes our general algorithm to simulate the surface array response. The detailed study of  $r_{opt}$  is presented in section 3. The energy determination method and the results about the energy spectrum are shown in section 4. Our conclusions are given in section 5.

## 2 Algorithm

A previous version of our algorithm has been presented in [17]. We use a numerical approach to simulate the EAS detection in a surface array. Our toy-detector is an infinite array of equally spaced surface detectors, located at the vertexes of a triangular grid of variable spacing. We can modify the detector separations, and analyze primary energies between  $10^{17}$  and  $10^{21}$  eV

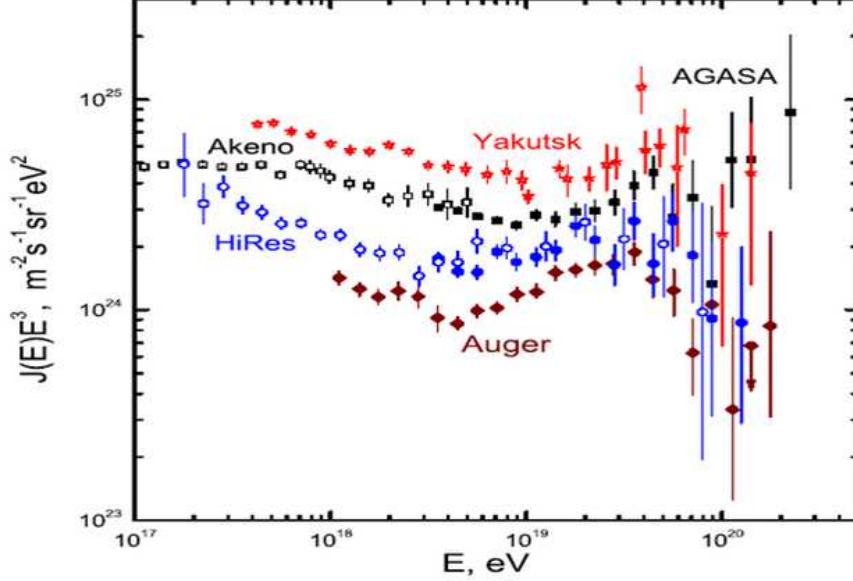


Fig. 1. Energy Spectrum measured by different experiments. The compilation is from V. Berezhinsky, with the HiRes and PAO results shown in the 30<sup>th</sup> International Cosmic Ray Conference, Mérida, México, 2007. The vertical axis is multiplied by  $E^3$  to emphasize the spectral structure.

and zenith angles from 0 to 60 degrees. Azimuthal angles have been selected randomly.

Whenever we simulate a water Cherenkov detector, we assume that the true lateral distribution of the signal is best represented by a Nishimura-Kamata-Greisen (NKG) function [18] normalized at 1000 m in the same way as the reported Auger LDF [1]:

$$S(r_{km}, E_{EeV}, \theta) = \frac{7.53 E^{0.95} 2^{\beta(\theta)}}{\sqrt{1 + 11.8[\sec(\theta) - 1]^2}} \times r^{-\beta(\theta)} \times (1 + r)^{-\beta(\theta)} \quad (1)$$

where  $\beta(\theta) = 3.1 - 0.7\sec(\theta)$ . We use this LDF to simulate events for any given incoming direction and energy. For each shower, a core is randomly selected inside an elementary cell of the surface grid and use eq. 1 to assign signals to the stations. The expected signal at each station is then fluctuated with a Poissonian distribution whose mean is given by eq. 1, the "true" LDF. We impose as a trigger condition  $S(r) = 3.0$  VEM, i.e. the signal deposited by one vertical muon in an Auger water Cherenkov tank. Stations with signal  $S_i > S(0.2 \text{ km}, 1 \text{ EeV}, 0^\circ)$  are considered saturated and are excluded.

For the case of scintillators as those of the AGASA experiment, we use the AGASA LDF [5]:

$$\rho(r) = K \left( \frac{r}{r_M} \right)^{-1.2} \times \left( 1 + \frac{r}{r_M} \right)^{-(\eta(\theta)-1.2)} \times \left( 1 + \left( \frac{r}{1000\text{m}} \right)^2 \right)^{-0.6} \quad (2)$$

where  $r_M = 91.6 \text{ m}$  is the Moliere radius at AGASA altitude,  $\eta(\theta) = 3.84 - 2.15(\sec(\theta) - 1)$  and  $K$  is the shower size given by:

$$K(\theta, E_{\text{EeV}}) = 49.676 \times f_s(\theta) \times \left( 1 + \frac{600}{r_M} \right)^{\eta(\theta)-1.2} \times E^{1/1.03} \quad (3)$$

where  $f_s(\theta)$  is the attenuation curve as shown in eq. 6. In this case, the trigger condition is  $\Delta\rho/\rho \geq 0.5$ , while the saturation condition is analogous to the one before  $\rho_i > \rho(0.2 \text{ km}, 1 \text{ EeV}, 0^\circ)$ . Thereafter we proceed as in the previous case.

For each shower, the uncertainty in the reconstructed core position is accounted for by perturbing the *real* core position using a Gaussian distribution centered at that point. The standard deviation of this distribution is chosen in accordance with the uncertainty in core determination, which depends on the array geometry and primary energy, as estimated in reference [19]. The new core position simulates the *reconstructed* core.

In section 3 where we study the  $r_{opt}$  dependence on energy, zenith angle and array spacing. Since the exact functional form of the LDF function is not crucial [20] we use a generic LDF parametrization to fit the signals of the triggered stations:

$$\log S(r) = a_1 r^{-a_2} + a_3 \quad (4)$$

In section 4, we study the effects of  $r_{opt}$  on the determination of the spectrum in an AGASA-like experiment. In that case, we use eq. 2 to generate the signals at the scintillators, and fit the “observed” LDF using an equation of the form:

$$\log \rho(r) = a_1 - a_2 \log(r/r_M) - 0.6 \log(1 + (r/1000\text{m})^2) \quad (5)$$

which is formally equivalent to eq. 2 for  $r \gg r_M$ .

For any given shower, the following procedure is used to obtain its actual optimum distance  $r_{opt}$ . The uncertainty in the true position of the core is accounted for by shifting 50 times the *reconstructed* core using a Gaussian distribution. This Gaussian distribution is centered at the position of the originally reconstructed core and with the same standard deviation used before. For each new

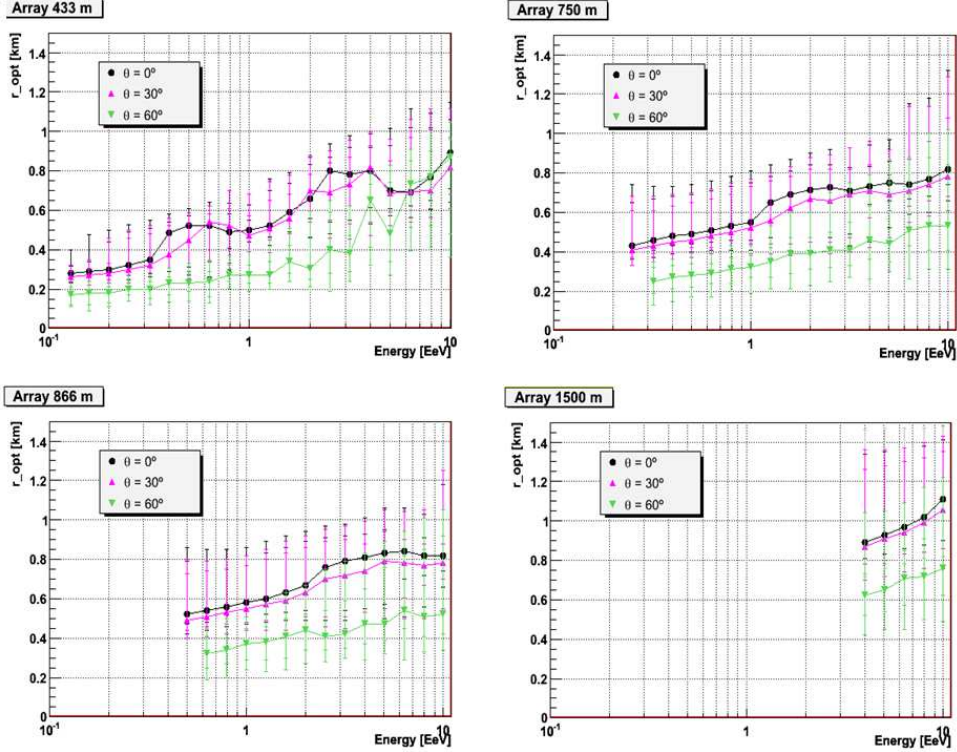


Fig. 2.  $r_{opt}$  vs energy for different array spacing and zenith angle. The error bars represent the 68% and 95% C.L.

core position, the LDF fit is performed using eq. 4 or 5, depending of the detector type under consideration as explained above, and the  $r_{opt}$  value is defined as the point for which the interpolated signal dispersion goes through a minimum.

### 3 $r_{opt}$ dependence on array spacing, energy and zenith angle.

We consider here detector separations of 433, 750, 866 and 1500 m, as well as primary energies varying from  $10^{17}$  to  $10^{19}$  eV. We use eq. 1 to generate the signals and eq. 4 to fit the LDF. Figures 2, 3 and 4 show the dependence of  $r_{opt}$  on primary energy, zenith angle and detector separation respectively. The relation between  $r_{opt}$  and energy is almost linear. The value of  $r_{opt}$  is almost independent of zenith angle for  $\theta \lesssim 30^\circ$ , but decreases strongly with increasing zenith angle for larger  $\theta$ . This result comes from the fact that, for large angles, the array spacing appears smaller from the viewing perspective of the shower front and, therefore,  $r_{opt}$  decreases as obtained. For example the results are in agreement with the values adopted by Auger (separation of 1.5 km and  $r_{opt} = 1000$  m).

The effect of saturated stations, can be seen more easily from Fig. 5, where

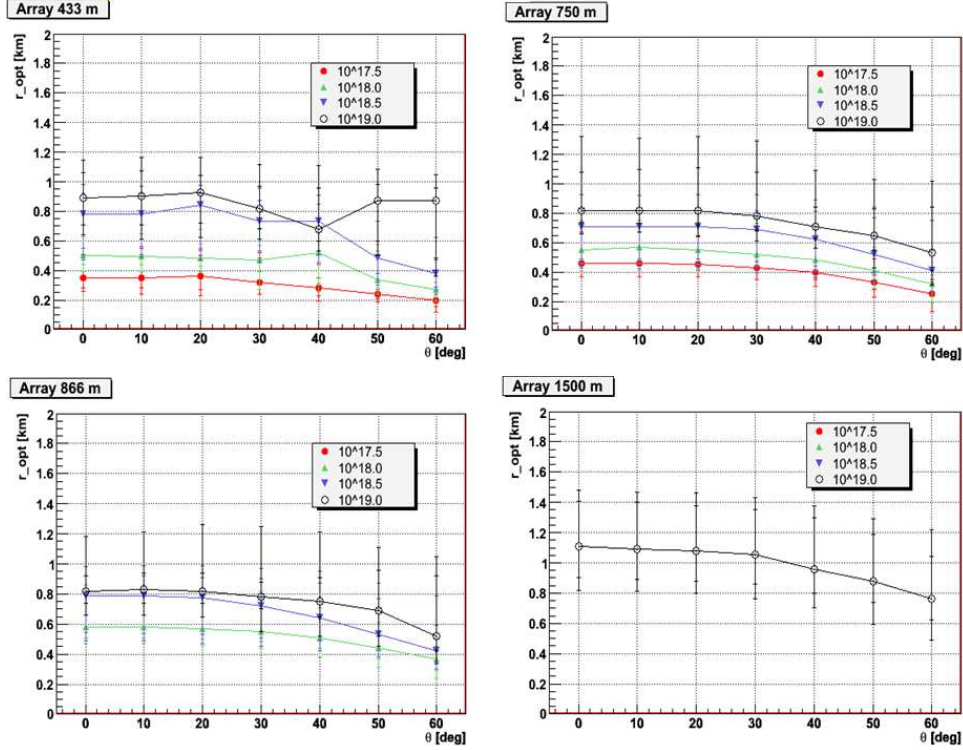


Fig. 3.  $r_{opt}$  vs zenith angle for different array spacing and energies. The error bars represent the 68% and 95% C.L.

we select events with “real“ cores located at less than 150 m from a station. It can be seen that, with the exception of the smaller separation array,  $r_{opt}$  is almost constant and its value is close to the detector separation for any given array. The reason for this is that the first stations that do not saturate are all clustered on a ring with a radius equal to the detector separation distance and, therefore, it is there that the several fits to the LDF also cluster independently of the shower energy. The effect is much less marked for inclined showers, as the relative number of triggered stations increases with zenith angle, the probability of saturation gets progressively smaller due the larger air mass that the showers have to traverse to reach the detector and the footprint on the ground gets elongated. In the case of the array at 433 m spacing,  $r_{opt}$  is approximately constant and equal to the array spacing for energies below  $2 \times 10^{18}$  eV. However, at larger energies, the whole first ring of triggered stations is saturated and, consequently,  $r_{opt}$  jumps to a new plateau with a value approximately equal to twice the array spacing, i.e., the radius of the first ring of non-saturated stations. At very low energy,  $E < 2 \times 10^{17}$  eV,  $r_{opt}$  increases steadily with energy, and this is due to the fact that in this limit there is almost no saturation.

The most important point to note is the dependence of  $r_{opt}$  with primary energy and zenith angle and its considerable dispersion, so that fixing its value could compromise energy estimation.



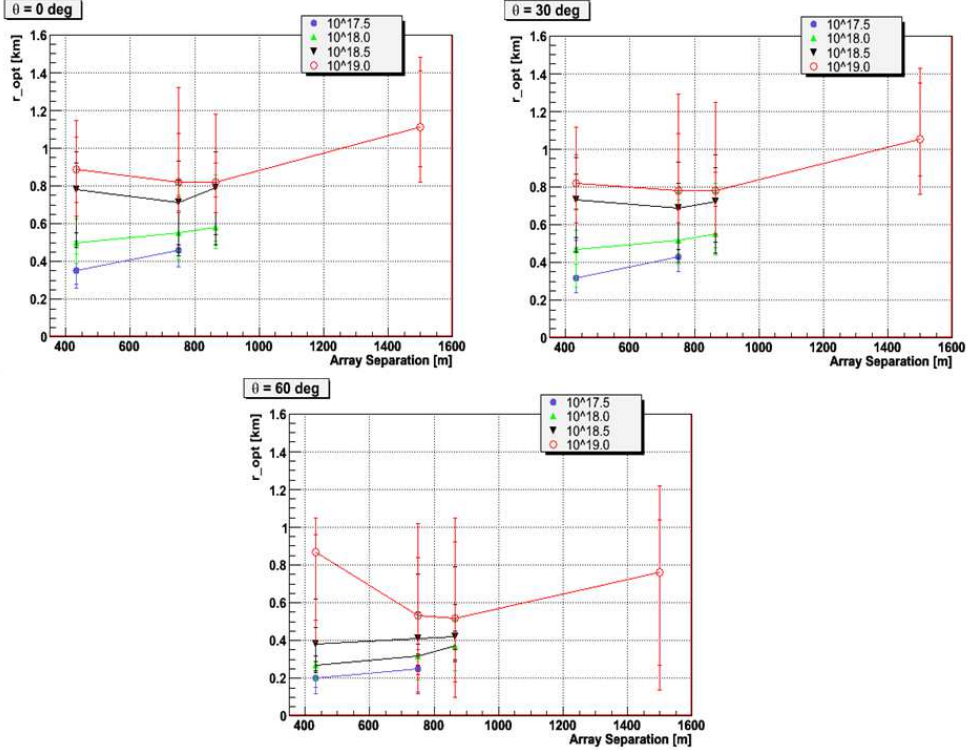


Fig. 4.  $r_{opt}$  vs array spacing for different zenith angle and energies. The error bars represent the 68% and 95% C.L.

#### 4 Influence of $r_{opt}$ in energy spectrum determination

In this section we analyze the effect of adopting a fix value for  $r_{opt}$ , instead of a shower-specific  $r_{opt}$ , on the determination of the energy spectrum. We generate signals with eq. 2 and use the eq. 5 to fit the “observed” LDF. We emulate a detector similar to AGASA, i.e., a separation between stations of 1 km and a total of 230.000 events which is, approximately, the same statistics used for constructing the spectrum showed in Fig.1. We analyze two case: (i) a perfect power law input spectrum with spectral index  $-3.0$  from  $10^{18.0}$  to  $10^{20.1}$  eV, and (ii) a more structured spectrum which extends from  $10^{17.7}$  to  $10^{21.0}$  eV, possesses an ankle, a GZK-cut-off, and is exposure-limited at low energy. In both cases, the angular distribution is randomly extracted from an isotropic distribution with a maximum zenith angle of  $45^\circ$ . We describe first the procedure by which the primary energy is obtained and, after that, the results are shown and discussed.

We want to emphasize that the results obtained in this section would not directly affect the Auger spectrum obtained with its surface array, because of the use of hybrid events for the energy calibration (details can be seen in ref. [4]).



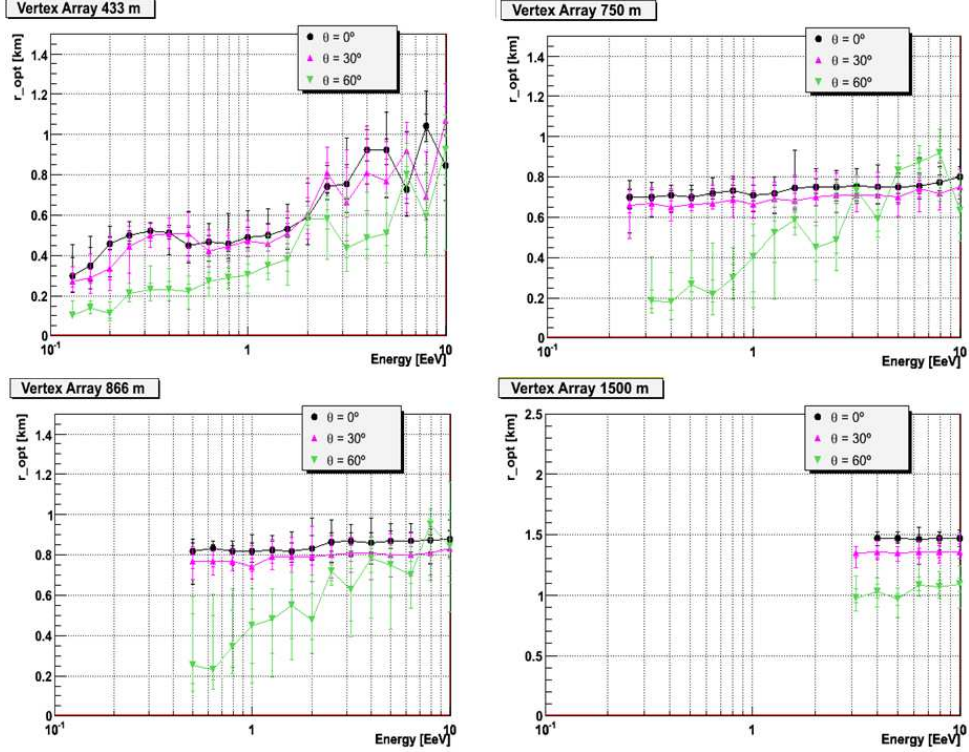


Fig. 5.  $r_{opt}$  vs energy for different array spacing and zenith angle for events with core close to a station. The error bars represent the 68% and 95% C.L.

#### 4.1 Energy Determination

We reconstruct shower energy using two different methods as is explained next.

First, we use the AGASA procedure [5] to determine the energy from the interpolated signal at 600 m. Since an inclined air shower traverses more atmosphere than a vertical one, the AGASA group transformed the shower density  $\rho_\theta(600)$  observed at zenith angle  $\theta$  into  $\rho_0(600)$ , the corresponding value to a vertical shower. The corresponding attenuation curve is:

$$\begin{aligned}
 \rho_\theta(600) &= \rho_0(600) \times f_s(\theta) \\
 &= \rho_0(600) \times \exp \left[ -\frac{X_0}{\Lambda_1} (\sec\theta - 1) - \frac{X_0}{\Lambda_2} (\sec\theta - 1)^2 \right] \quad (6)
 \end{aligned}$$

where  $X_0 = 920 \text{ g/cm}^2$ ,  $\Lambda_1 = 500 \text{ g/cm}^2$  and  $\Lambda_2 = 594 \text{ g/cm}^2$  for showers with  $\theta \leq 45^\circ$ . The uncertainty in  $\rho_0(600)$  due to this transformation is estimated at the level of  $\pm 5\%$ . The conversion formula reported by AGASA that relates  $\rho_0(600)$  with energy is:

$$E = 2.21 \cdot 10^{17} \times \rho_0(600)^{1.03} eV \quad (7)$$

where different hadronic interaction models and simulation codes have been considered. We use eq. 7 to estimate the energy from the signal at 600 m.

In the second method we use the signal at  $r_{opt}$  to estimate the shower energy. Once the  $\rho(r_{opt})$  has been determined as explained in section 2, the shower size is obtained from eq. 2 and the primary energy from eq. 3. In fact, parametrization of shower size as shown in eq. 3 has been obtained from eq. 2 and eq. 7.

#### 4.2 Results and discussion

First, we used a flat spectrum from  $10^{17.7}$  to  $10^{21.0}$  eV to calculate the real energy distribution function of events contributing to each reconstructed energy bin, both for  $r(600)$  and  $r_{opt}$ . The corresponding 68% and 95% confidence levels at the low (**L**) and high (**H**) energy sides for each distribution are shown in Fig. 6.a-f. For a Gaussian distribution, it is expected that  $\sigma_H/\sigma_L = 1$  (for both C.L. showing the perfect symmetry of the distribution) and  $\sigma_{95}/\sigma_{68} = 2$  (for the low and high sides). This is nearly true for the energies estimated using  $r_{opt}$  (Fig. 6.a-b). However, the distributions are skewed for  $r(600)$  (Fig. 6.c-d). This behavior is somehow improved if the events that have saturated stations are discarded (Fig. 6.e-f), although at the high cost of severely decreasing high energy statistics, for example around 80% of events at  $10^{19}$  eV (Fig. 6.h).

Finally, we compare the median of the distributions in order to assess any possible bias in each case. The bias is lower than 1% as seen in Fig. 6.g. In both cases the bias is negligible. Note that, in order to avoid border effects, the bins at both ends of the spectrum have been removed from the figures.

Fig. 7 compares both reconstruction techniques when applied to a power law spectrum ranging from  $10^{18.0}$  to  $10^{20.1}$  eV. The slope of the spectrum is better reconstructed using  $\rho(r_{opt})$  than  $\rho(600)$ . Again a considerable improvement is obtained by neglecting events with saturated stations, but at a high statistical cost. Furthermore, using  $\rho_0(600)$  around 11% of the events are reconstructed outside the input bounds (most of them are events in the lower energy bins). However, in the case of  $\rho(r_{opt})$  these are reduced to  $\sim 1\%$  of the events.

It is important to emphasize two points. First, in both cases, using  $\rho_0(600)$  or  $\rho(r_{opt})$ , the  $\chi^2/ndof$  of the corresponding fits are very good. Second, in the case of  $\rho_0(600)$ , the energy reconstruction is very bad for events with one or more saturated stations and energy below  $10^{18.5}$  eV and so they were rejected to improve reconstruction. With more energetic primaries this problem does

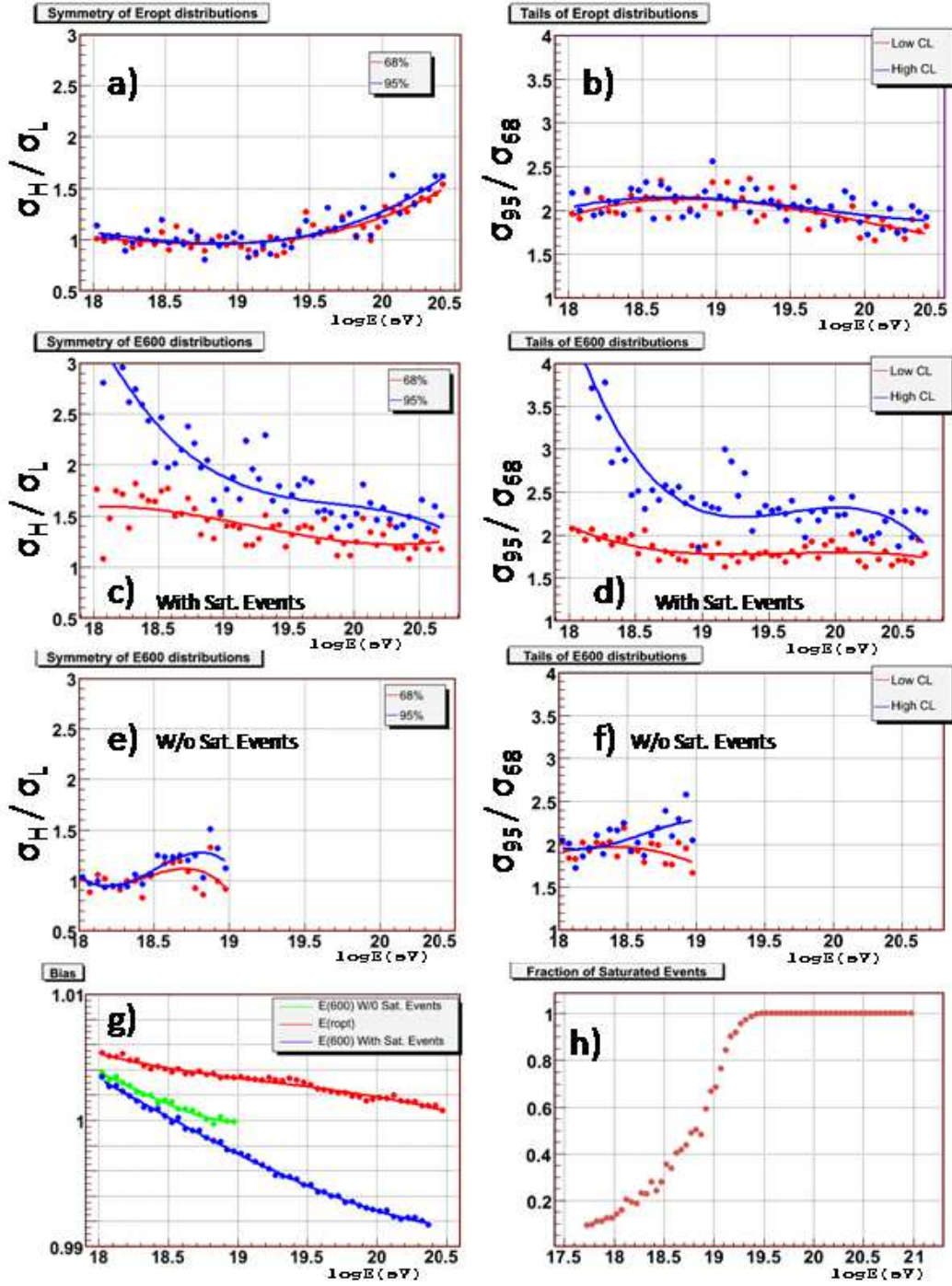


Fig. 6. From a) to f): First row is for  $E(r_{opt})$ , the second row is for  $E(r(600))$  with events with saturated stations included and the third row is for  $E(r(600))$  but without these events. The left panels assess the symmetry of the distributions comparing their high and low sides (Gaussian  $\sigma_H/\sigma_L = 1$ ). The right panels assess the existence and magnitude of tails in the energy distributions by comparing their C.L. at 68% and 95% (Gaussian  $\sigma_{95}/\sigma_{68} = 2$ ). (g) reconstructed energy bias. (h) fraction of events with at least one saturated station as a function of energy.

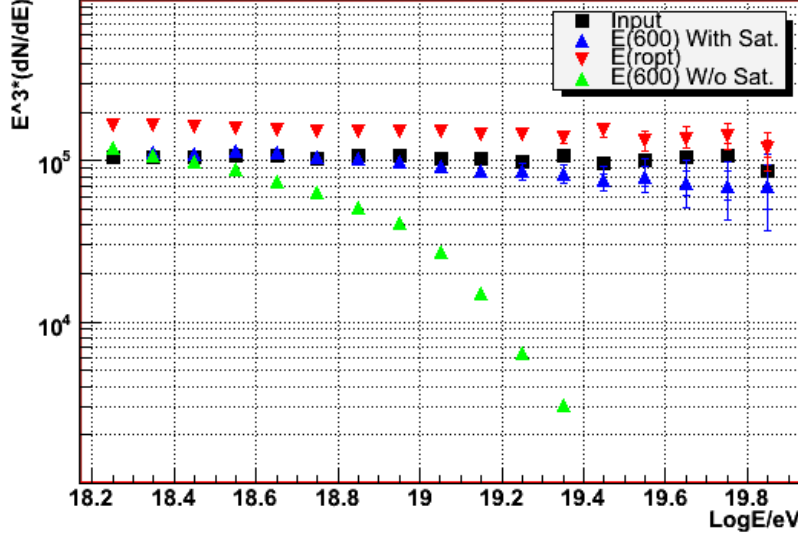


Fig. 7. Input spectrum (black squares) with the same statistic as AGASA. Reconstructed spectra obtained with  $\rho_0(600)$  (blue upward triangles) and  $S(r_{opt})$  (red downward triangles) as energy estimators. The spectrum obtained using  $\rho_0(600)$  but rejecting saturated events is depicted in green. The vertical axis is multiplied by  $E^3$ . Error bars are the C.L. at 68 and 95% obtained with 112 spectrums.

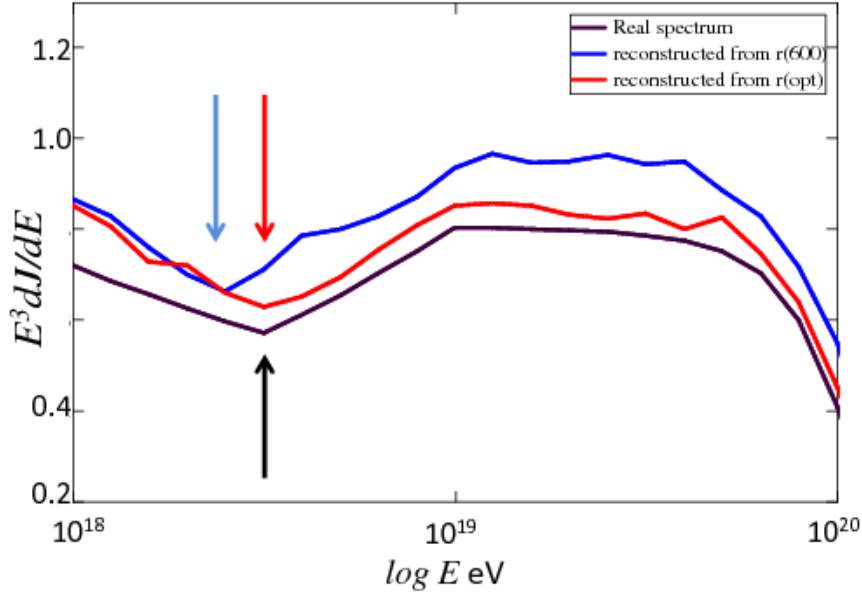


Fig. 8. Input structured spectrum (black) and the reconstructed spectra using  $\rho_0(600)$  (blue) and  $\rho(r_{opt})$  (red) as energy estimators. Note the position of the ankle and the sharpness and location of the GZK transition. As explain in the text this result does not directly apply to hybrid experiments like Auger.

not exist because the number of triggered stations increases. If  $\rho(r_{opt})$  is used instead, there are no problems with events with saturated stations at any energy, highlighting a major advantage of the latter method. Again the bins at both ends has been removed to avoid border effects.

Finally Fig. 8 shows the effects of both energy reconstructions when applied to a realistically structured spectrum (black curve), with an ankle and a GZK modulation, observed by an array with tanh acceptance that attains full efficiency  $\leq 10^{18}$  eV. The input spectrum has been convoluted with an asymmetric generalized Gaussian function (AGG) defined as:

$$P_{AGG}(y) = \begin{cases} \left(\frac{c\gamma_a}{\Gamma(1/c)}\right) \exp\{-\gamma_l^c[-(y-\mu)]^c\} & \text{if } y < \mu \\ \left(\frac{c\gamma_r}{\Gamma(1/c)}\right) \exp\{-\gamma_r^c[(y-\mu)]^c\} & \text{if } y \geq \mu \end{cases}$$

where,

$$\gamma_a = \frac{1}{\sigma_l + \sigma_r} \left(\frac{\Gamma(3/c)}{\Gamma(1/c)}\right)^{1/2} \quad \gamma_l = \frac{1}{\sigma_l} \left(\frac{\Gamma(3/c)}{\Gamma(1/c)}\right)^{1/2} \quad \gamma_r = \frac{1}{\sigma_r} \left(\frac{\Gamma(3/c)}{\Gamma(1/c)}\right)^{1/2}$$

and  $\sigma_l^2$  and  $\sigma_r^2$  are the variances of the left and right sides of the probability density function respectively and  $\Gamma(x)$  is the Gamma function. If  $\sigma_l^2 = \sigma_r^2$  it is symmetric. In the case  $\sigma_l^2 = \sigma_r^2$  and  $c = 2$ , AGG coincides with the Gaussian model, and for  $c = 1$  it represents the Laplacian distribution. By fixing the values of  $\sigma_l$ ,  $\sigma_r$ ,  $\mu$  and  $c$ , the AGG can be used to acceptably reproduce the asymmetries present on the distribution functions mapping real to reconstructed energy for both techniques,  $r(600)$  and  $r_{opt}$  over the whole energy range of interest. The results are shown in Figure 8. It can be seen that, while the  $\rho(r_{opt})$  method fairly reproduces the impinging spectrum, the  $\rho_0(600)$  method changes the ankle position and smooths the GZK transition slightly shifting its start to lower energies.

## 5 Conclusions

In this work we have shown the advantages of using the optimum distance for each individual shower, instead of a fixed value, as it is generally done in surface arrays. We studied the dependence of  $r_{opt}$  with energy, zenith angle and array spacing, showing that they are not negligible and that an important dispersion exists. We also reconstructed both, a featureless power law spectrum and one with considerable structure, and demonstrate that using  $r_{opt}$  for each shower improves the reliability of the calculated spectrum. Using a fixed distance to estimate the energy may change the slope of the spectrum, the position of the ankle and smooth the GZK transition. Additionally, the  $r_{opt}$  strategy maximizes the number of events suitable for spectral reconstruction

for a given exposure and reduces, at the same time, possible biases originated by the implementation of algorithms designed to recover saturated signals.

## 6 Acknowledgements

All the authors have greatly benefited from their participation in the Pierre Auger Collaboration and its profitable scientific atmosphere. G. Ros thanks the Comunidad de Madrid for a F.P.I. fellowship and the ALFA-EC funds, in the framework of the HELEN project. G. Medina Tanco also acknowledges the support of the HELEN project. This work is partially supported by Spanish MINISTERIO DE EDUCACIÓN Y CIENCIA under the projects FPA2006-12184-C02-02, CAM/UAH2005/071, CM-CCG06-UAH/ESP-0397, CSD2007-00042, FPA2006-12184-C02-01 and CM-UCM 910600, and Mexican PAPIIT-UNAM through grants IN115707 and IN115607 and CONACyT through grants 46999-F and 57772. G. Ros also thanks to the Inst. de Ciencias Nucleares, UNAM, for its hospitality during several stays.

## References

- [1] The Pierre Auger Collaboration. Nucl. Instr. And Meth., **523**, 50-95 (2004). (See also [www.auger.org.ar](http://www.auger.org.ar)).
- [2] A. M. Hillas. Acta Phys. Acad. Sci. Hung., 29, Suppl. 3, 355 (1970).
- [3] D. Newton et al. astro-ph/0608118.
- [4] The Pierre Auger Collaboration. Proc. 30th International Cosmic Ray Conference, Mérida, México, 2007. arXiv:0706.2096.
- [5] Takeda et al. Astroparticle Physics **19**, 447-462 (2003).
- [6] A.A. Ivanov et al. Nucl. Phys. B **122**, 226-230 (2003).
- [7] T. Abu-Zayyad et al. Astrophys. J. **557**, 686 (2001).
- [8] M. Ave et al. Proc. 27th International Cosmic Ray Conference, Hamburg, Germany, vol. **I**, 2001, p.381. astro-ph/0112253.
- [9] HiRes Collaboration. Proc. 30th International Cosmic Ray Conference, Mérida, México, 2007. astro-ph/0706.1248.
- [10] A. M. Hillas. Nucl. Phys. B **136**, 139 (2004) .
- [11] D. Allard et al. astro-ph/0505566.
- [12] V.S. Berezhinsky et al. Phys. Lett. B **612**, 147 (2005). astro-ph/0502550.

- [13] G. A. Medina-Tanco, Proc. Mexican School on Astrophysics 2005 (EMA2005), astro-ph/0607543.
- [14] G. A. Medina-Tanco, Pierre Auger Collaboration, arXiv:0709.0772
- [15] C. De Donato and G. A. Medina-Tanco Proc. 30th ICRC, Mérida, México, 2007. arXiv:0708.0203.
- [16] C. De Donato and G. A. Medina-Tanco in preparation, 2008.
- [17] G. A. Medina-Tanco et al. Proc. 29th International Cosmic Ray Conference Pune, **7**, 43-46 (2005).
- [18] K. Greisen. Progress in Cosmic Ray Physics, vol. **3**, (1956).
- [19] M.C.Medina et al. Nucl. Inst. and Meth. A **566**, 302-311 (2006). astro-ph/0607115.
- [20] The Pierre Auger Collaboration. Proc. 29th International Cosmic Ray Conference, Pune, **7**, 291-294 (2005).